

Myofibroblast dedifferentiation proceeds via distinct transcriptomic and phenotypic transitions

Sean M. Fortier,¹ Loka R. Penke,¹ Dana King,² Tho X. Pham,³ Giovanni Ligresti,³ and Marc Peters-Golden¹

¹Division of Pulmonary and Critical Care Medicine and ²BCRF Bioinformatics Core, University of Michigan, Ann Arbor, Michigan, USA. ³Department of Medicine, Boston University School of Medicine, Boston, Massachusetts, USA.

Myofibroblasts are the major cellular source of collagen, and their accumulation – via differentiation from fibroblasts and resistance to apoptosis – is a hallmark of tissue fibrosis. Clearance of myofibroblasts by dedifferentiation and restoration of apoptosis sensitivity has the potential to reverse fibrosis. Prostaglandin E₂ (PGE₂) and mitogens such as FGF2 have each been shown to dedifferentiate myofibroblasts, but – to our knowledge – the resultant cellular phenotypes have neither been comprehensively characterized or compared. Here, we show that PGE₂ elicited dedifferentiation of human lung myofibroblasts via cAMP/PKA, while FGF2 utilized MEK/ERK. The 2 mediators yielded transitional cells with distinct transcriptomes, with FGF2 promoting but PGE₂ inhibiting proliferation and survival. The gene expression pattern in fibroblasts isolated from the lungs of mice undergoing resolution of experimental fibrosis resembled that of myofibroblasts treated with PGE₂ in vitro. We conclude that myofibroblast dedifferentiation can proceed via distinct programs exemplified by treatment with PGE₂ and FGF2, with dedifferentiation occurring in vivo most closely resembling the former.

Introduction

Fibrosis is the consequence of a disordered and pathologic host response to tissue injury that affects all organ systems and is associated with a high morbidity and mortality (1, 2). Idiopathic pulmonary fibrosis (IPF) is a severe and progressive lung disease characterized by parenchymal scarring that leads to architectural distortion, respiratory failure, and death (3). The ultimate effector cell of fibrotic disorders is the myofibroblast — a large stellate-shaped cell with numerous exocytotic vesicles, focal adhesions, and stress fibers composed of α -smooth muscle actin (α SMA). Lung myofibroblasts originate predominantly from resident fibroblasts whose further phenotypic differentiation is driven by profibrotic mediators, such as TGF- β . These cells promote fibrosis and tissue stiffness by virtue of their capacity to secrete abundant quantities of various extracellular matrix proteins such as collagens, elastin, and fibronectin and via their contractile function (4, 5). An additional important characteristic feature of myofibroblasts in IPF and other fibrotic disorders is their resistance to apoptosis, which contributes to their accumulation in involved tissues (6, 7). This accumulation of myofibroblasts contrasts with their eventual clearance during normal wound healing, thus allowing fibrosis to persist and progress (8).

Patients diagnosed with IPF usually come to clinical attention only after fibrosis is already established. Unfortunately, current therapies fail to reverse established fibrosis, in part because they do not eliminate the activated myofibroblasts that have accumulated. Although myofibroblasts were historically considered to be terminally differentiated cells, their capacity for dedifferentiation, defined as the loss of α SMA stress fibers, is now well recognized and has been implicated as being necessary for fibrosis resolution (9).

The 2 substances best established to promote dedifferentiation are the soluble mediators prostaglandin E₂ (PGE₂) (10–12) and mitogens such as FGF2 (13, 14). However, it is currently unclear how these 2 categories of molecules — which signal in entirely different ways — orchestrate the phenotypic transition of myofibroblasts. In the present study, we investigated this by performing mechanistic, RNA sequencing (RNA-seq), and functional studies on PGE₂- and FGF2-treated human lung myofibroblasts examined in parallel. While treatment with PGE₂ and FGF2 both downregulated hallmark fibrotic genes such as α SMA, collagen I, and fibronectin, they did so by generating distinct transitional cellular phenotypes, characterized by unique gene programs with differing capacities for proliferation and apoptosis. Finally, the gene signatures defined by RNA-seq of fibroblasts isolated from the lungs of young mice with resolving

Conflict of interest: The authors have declared that no conflict of interest exists.

Copyright: © 2021, Fortier et al. This is an open access article published under the terms of the Creative Commons Attribution 4.0 International License.

Submitted: October 7, 2020

Accepted: February 4, 2021

Published: March 22, 2021

Reference information: *JCI Insight*. 2021;6(6):e144799.
<https://doi.org/10.1172/jci.insight.144799>.

bleomycin-induced fibrosis were compared with those of myofibroblasts dedifferentiated in vitro and were found to more closely resemble those observed in cells treated with PGE₂ than with FGF2.

Results

PGE₂ utilizes the EP2/cAMP/PKA pathway to dedifferentiate myofibroblasts, whereas FGF2 requires MEK/ERK. The abilities of PGE₂ and FGF2 to elicit myofibroblast dedifferentiation have been studied individually but have not previously been directly compared. As depicted in the experimental scheme in Figure 1A, myofibroblasts were first established by treating normal adult human lung fibroblasts with TGF-β for 48 hours in serum-free medium, followed by subsequent addition of PGE₂ or FGF2 to initiate dedifferentiation. We initially evaluated the effects of each treatment on the characteristic fibrosis-associated protein and myofibroblast marker αSMA. As expected, myofibroblasts expressed much higher levels of αSMA protein than did fibroblasts. Moreover, both PGE₂ and FGF2 reduced the expression of αSMA protein at 5 days. Notably, PGE₂ elicited a greater decline in αSMA (Figure 1B). In parallel with this global decline in αSMA protein, its assembly into stress fibers — an essential component of the myofibroblast contractile machinery — was also disrupted by treatment with PGE₂ and FGF2 (Figure 1C). These results confirm that PGE₂ and FGF2 each have the capacity to dedifferentiate myofibroblasts.

We confirmed that they elicited parallel reductions in αSMA mRNA (*ACTA2*), as well as the highly expressed myofibroblast genes collagen I (*COL1A1*) and fibronectin (*FNI*), when analyzed at 24 hours and 48 hours, respectively (Figure 1, D and E). These time points were selected based on observed differences in the dedifferentiation kinetics triggered by the 2 mediators in pilot experiments. It is notable that this shared outcome for both mediators occurs despite marked differences in their molecular identity, the characteristics of their cognate receptors, and second messenger signaling cascades. PGE₂ is a prostaglandin lipid mediator known to interact with 4 E-prostanoid GPCRs (EP1–EP4), which signal through the second messengers cAMP or calcium (15). In contrast, FGF2 signals through a receptor tyrosine kinase affecting multiple downstream pathways, including PI3K, protein kinase B (AKT), and the MAPKs (16). We therefore investigated the signaling pathways involved in PGE₂- and FGF2-mediated myofibroblast dedifferentiation. We have shown previously that PGE₂ prevents TGF-β-induced fibroblast differentiation mainly by activation of the EP2 receptor, which stimulates adenylyl cyclase to increase production of intracellular cAMP and activate protein kinase A (PKA) (17–19). Accordingly, we examined the abilities of these same signaling pathway components of PGE₂ to elicit myofibroblast dedifferentiation. Both butaprost, a PGE₂ analog that specifically activates EP2, and forskolin, a direct activator of adenylyl cyclase, reduced levels of *ACTA2*, *COL1A1*, and *FNI* (Figure 1, D and E). cAMP can act via 2 effector proteins, PKA and the guanine nucleotide exchange protein activated by cAMP (Epac). A cAMP analog that selectively activates PKA (6-BNZ cAMP) was also capable of dedifferentiation, whereas one that selectively activates Epac (8-pCPT cAMP) was not. Next, we explored FGF2 signaling and found that its ability to reduce expression of αSMA and collagen I was overcome by inhibition of the MEK/ERK pathway (Figure 1E and Supplemental Figure 1A; supplemental material available online with this article; <https://doi.org/10.1172/jci.insight.144799DS1>) but not by inhibition of the MAPKs p38 or JNK, or by inhibition of AKT (Supplemental Figure 1B). The distinctiveness of the signaling pathways by which the 2 mediators exert their effects is underscored by the fact that the effects of PGE₂ were not abolished by treatment with the ERK inhibitor U0126 (Supplemental Figure 1C). The modest reduction in *FNI* by FGF2 was not abolished by inhibition of MEK/ERK, p38, JNK, or AKT (Supplemental Figure 1D). The signaling mechanisms by which PGE₂ and FGF2 promote myofibroblast dedifferentiation are summarized in Figure 1F.

Transcriptome profiling of PGE₂- and FGF2-treated myofibroblasts via RNA-seq. Although we previously utilized microarray analysis to describe the transcriptomic effects of PGE₂ in TGF-β-elicited myofibroblasts (12), that analysis lacked a comprehensive examination of noncoding RNAs (ncRNAs), as well as a comparison with the effects of FGF2. The fact that PGE₂ and FGF2 led to myofibroblast dedifferentiation by exploiting different signaling pathways provided the impetus to undertake a more comprehensive examination that might reveal differences in the transitional cell phenotypes that they elicit. We interrogated this possibility using RNA-seq to characterize genome-wide transcriptomic changes in myofibroblasts treated with either PGE₂ or FGF2. We sought to characterize early and comparable phases of the phenotypic transition promoted by PGE₂ and FGF2. The time point arbitrarily chosen for analysis was that which yielded an approximately 50% reduction in *ACTA2*, determined to be 6 hours for PGE₂ and 24 hours for FGF2 (Figure 2A). Each treatment condition was paired with a time-matched untreated myofibroblast control, and all analyses were performed in triplicate cultures. A total of 17,903 distinct RNA transcripts (excluding small RNAs) was detected. A high

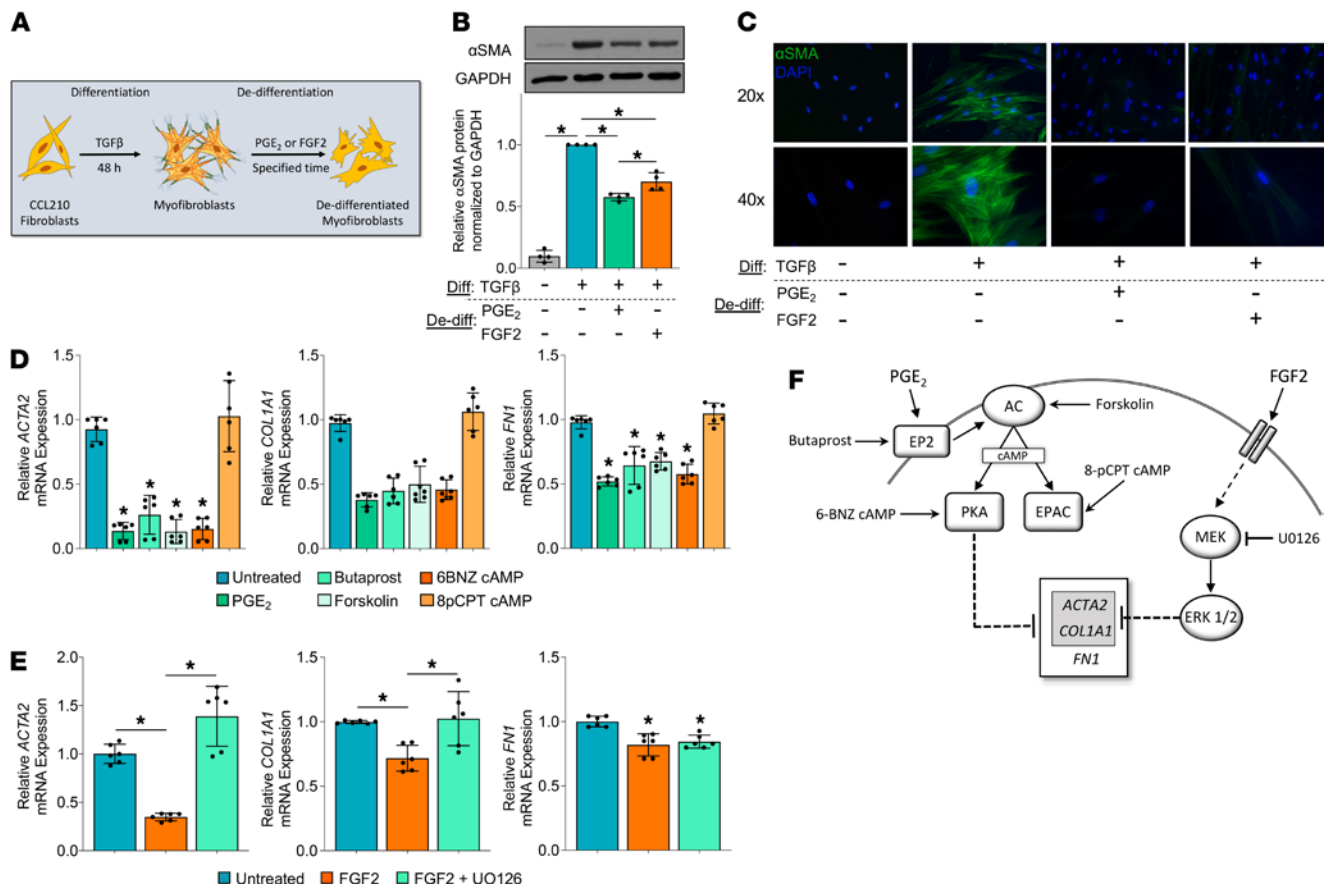


Figure 1. PGE₂ and FGF2 dedifferentiate established myofibroblasts via distinct signaling pathways. (A) Experimental scheme depicting myofibroblast differentiation of CCL210 fibroblasts with TGF-β (2 ng/mL) for 48 hours, followed by dedifferentiation with PGE₂ (1 μM) or FGF2 (50 ng/mL). (B) αSMA protein expression measured by Western blot analysis 5 days following treatment with PGE₂ or FGF2 compared with untreated fibroblast and myofibroblast controls. The histogram depicts mean densitometry values. (C) αSMA stress fibers identified by immunofluorescence microscopy using anti-αSMA antibody and FITC-conjugated secondary antibody. Nuclei are stained with DAPI. (D) Relative ACTA2, COL1A1, and FN1 expression by qPCR in myofibroblasts treated for 24 hours with PGE₂ (1 μM), the EP2 agonist butaprost (500 nM), the adenylyl cyclase activator forskolin (500 nM), the PKA specific cAMP analog 6-BNZ cAMP (2 mM), or the Epac specific cAMP analog 8-pCPT cAMP (2 mM). (E) Relative ACTA2, COL1A1, and FN1 expression by qPCR in myofibroblasts treated for 48 hours with FGF2 (50 ng/mL) with and without the MEK/ERK inhibitor UO126 (20 μM). (F) Schematic detailing PGE₂ signaling cascade via the EP2 receptor and FGF2 signaling through FGF2R via MEK/ERK. PKA mediates the reduction in ACTA2, COL1A1, and FN1 elicited by PGE₂, while MEK/ERK mediates the reduction in ACTA2 and COL1A1 elicited by FGF2. Relative fold changes of indicated genes measured by qPCR are normalized to GAPDH. Data are presented as mean ± SEM. Data points in B represent individual replicate samples from 4 separate experiments. Data points in D and E represent paired replicate samples from 3 experiments. Lines indicate conditions being compared. *P < 0.05, compared with untreated myofibroblast, 1-way ANOVA. Diff, differentiation; De-diff, dedifferentiation; AC, adenylyl cyclase.

degree of concordance was observed among the triplicate samples from each treatment condition (Supplemental Figure 2). PGE₂ differentially regulated 3105 genes, and FGF2 differentially regulated 1720 genes, as compared with their corresponding time-matched untreated controls. Of these, PGE₂ upregulated 1521 genes and downregulated 1584, whereas FGF2 upregulated 878 and downregulated 842 (Figure 2B). PGE₂ exhibited higher log-fold changes among top-regulated mRNAs than did FGF2, with only 1 gene — *DEPPI1*, a regulator of autophagy (20) — shared among the top 25 genes up- or downregulated by both mediators (Supplemental Table 1). Despite their distinct actions, PGE₂ and FGF2 mutually regulated 716 genes in common (Figure 2C). Principle components analysis showed similar clustering between 6 and 24 hours untreated controls but showed marked differences between myofibroblasts treated with PGE₂ versus FGF2, as well as between each agent and the untreated controls (Figure 2D).

Effects of PGE₂ and FGF2 on myofibroblast signaling pathways and gene ontology. We employed KEGG pathway enrichment analysis to characterize and compare the gene expression patterns of the transitional cellular phenotypes evoked by treatment of myofibroblasts with PGE₂ and FGF2. Of the KEGG pathways included in our analysis, PGE₂ and FGF2 each enriched 46 pathways, 17 of which were shared (Supplemental Table 2). From these, we curated a list of pathways lacking disease specificity, extrapulmonary organ selectivity,

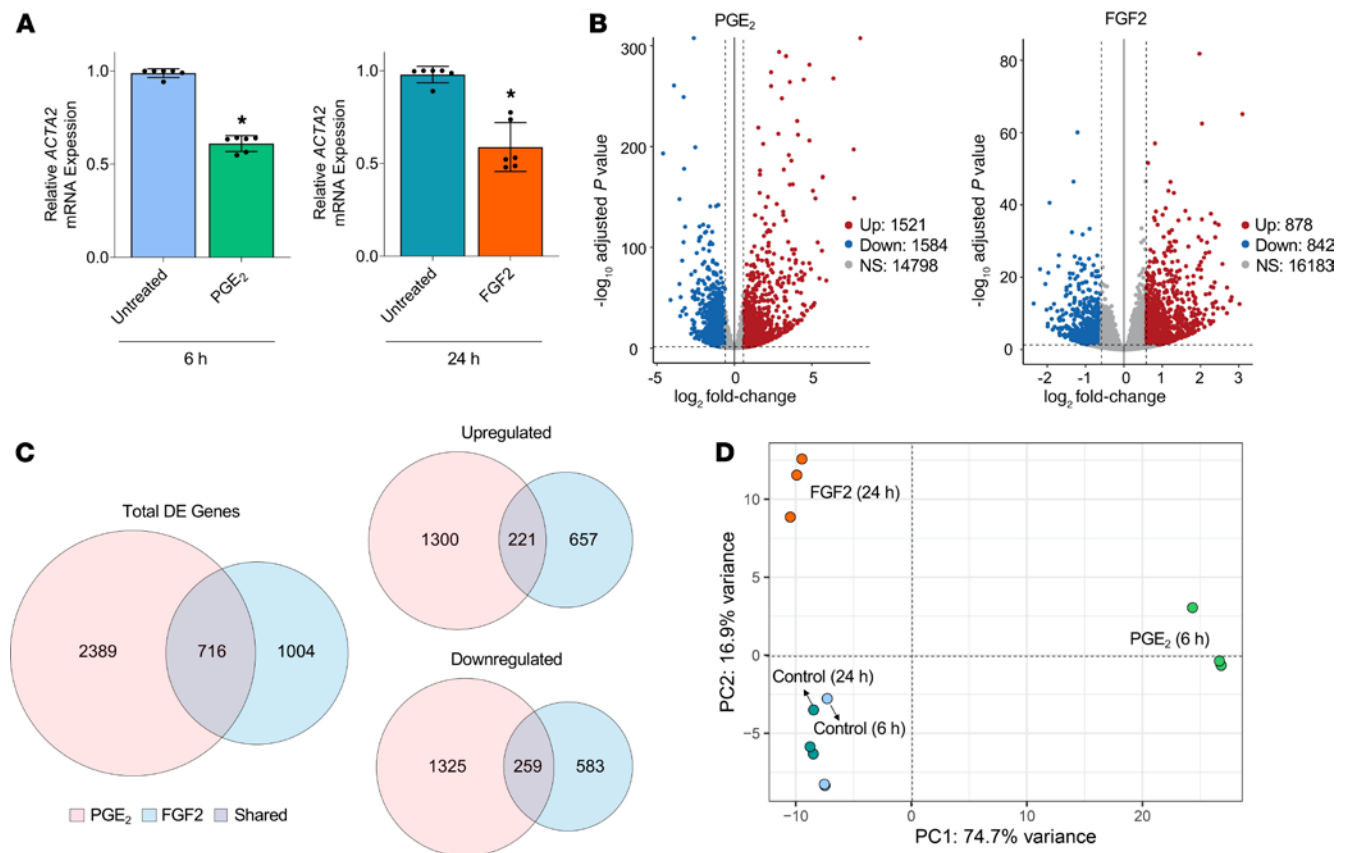


Figure 2. RNA-seq of established myfibroblasts treated with or without PGE₂ or FGF2. (A) qPCR analysis of RNA samples submitted for RNA-seq demonstrating approximately 50% reduction in *ACTA2* expression in myfibroblasts treated with PGE₂ (1 μM) or FGF2 (50 ng/mL) at 6 and 24 hours, respectively. Data points represent paired replicate samples from 3 experiments. Data are presented as mean ± SEM. **P* < 0.05, paired 2-tailed *t* test. (B) Volcano plots representing differential gene expression by log₂ fold change (x axis) and adjusted *P* value (y axis) of total RNA transcripts in PGE₂- and FGF2-treated myfibroblasts compared with time-matched controls. (C) Venn diagrams depicting the number of genes differentially expressed as well as those specifically upregulated and downregulated exclusively by PGE₂ (red), exclusively by FGF2 (blue), and by both mediators (gray). (D) Principal components analysis of the top 500 variably expressed genes in PGE₂- and FGF2-treated myfibroblasts and untreated time-matched controls. Relative fold changes of indicated genes measured by qPCR are normalized to *GAPDH*. Each colored circle denotes 1 of 3 replicate samples.

and functional redundancy (Table 1). Of these 22 remaining pathways, 14 were enriched by PGE₂, 16 were enriched by FGF2, and 8 pathways were enriched by both.

Among the pathways uniquely enriched by PGE₂ were MAPK and mTOR. Each has been shown to be involved in fibroblast biology in the context of pulmonary fibrosis (21, 22), with mTOR representing a potential target for antifibrotic therapy (23). In contrast, FGF2 predictably enriched cell cycle, apoptosis, and adhesion/anchoring pathways. Of particular interest were cellular functions enriched by both PGE₂ and FGF2, given the possibility that a common pathway downstream of cAMP/PKA and MEK/ERK may participate in mediating the dedifferentiating effects of each molecule. Indeed, both PGE₂ and FGF2 significantly impacted the fibrosis-associated pathways TGF-β, WNT, and PI3K-AKT. Notably, cAMP signaling was enriched by FGF2, as well as PGE₂ (Table 1).

As TGF-β plays an integral role in the initiation, maintenance, and progression of pulmonary fibrosis (24–26), we specifically examined and compared the regulation of known TGF-β-associated genes. Broadly, PGE₂ downregulated 21 TGF-β pathway genes, while FGF2 downregulated 10 (Figure 3). The canonical TGF-β effectors *SMAD3*, *SMAD7*, and *SMAD9* were downregulated by PGE₂, while FGF2 downregulated *SMAD7* and *SMAD9* without significant regulation of *SMAD3*. Notably, the NADPH oxidase gene *NOX4* — a central mediator of myfibroblast differentiation, ECM protein production, and contractility (27) — was downregulated by both effector molecules.

We next compared differentially expressed genes belonging to the remaining mutually enriched pathways (Figure 3). PGE₂ and FGF2 upregulated cytokines such as *IL6*, *IL11*, and *CCL2*, while downregulating *IL16* and *IL6R*. Interestingly, *SOCS3* — which opposes IL6 signaling by inhibiting JAK-STAT — was upregulated

Table 1. KEGG pathway enrichment following treatment with PGE₂ only, FGF2 only, or both PGE₂ and FGF2

	KEGG pathway	PGE ₂		FGF2	
		DE genes (Total)	Adjusted <i>P</i> value	DE genes (total)	Adjusted <i>P</i> value
Enriched by PGE ₂ only	MAPK signaling pathway	74 (total 263)	0.001	42 (total 251)	0.124
	cGMP-PKG signaling pathway	45 (total 140)	0.002	24 (total 131)	0.078
	Ras signaling pathway	59 (total 196)	0.006	28 (total 186)	0.436
	ErbB signaling pathway	20 (total 77)	0.008	11 (total 74)	0.323
	mTOR signaling pathway	33 (total 136)	0.013	12 (total 131)	1.000
	Apelin signaling pathway	36 (total 118)	0.018	17 (total 109)	0.194
Enriched by FGF2 only	Cell cycle	27 (total 123)	0.523	31 (total 122)	0.001
	p53 signaling pathway	20 (total 69)	0.096	18 (total 67)	0.003
	Cell adhesion molecules	20 (total 107)	0.750	23 (total 92)	0.003
	ECM-receptor interaction	12 (total 78)	0.815	16 (total 75)	0.025
	JAK-STAT signaling pathway	34 (total 115)	0.085	23 (total 105)	0.032
	Gap junction	22 (total 79)	0.089	18 (total 71)	0.034
	Histidine metabolism	4 (total 17)	0.667	6 (total 16)	0.038
Enriched by both PGE ₂ and FGF2	Tryptophan metabolism	12 (total 37)	0.132	10 (total 31)	0.014
	Cytokine-cytokine receptor interaction	61 (total 186)	1.07×10^{-5}	43 (total 154)	3.89×10^{-5}
	Hippo signaling pathway	54 (total 146)	1.59×10^{-5}	29 (total 136)	0.027
	cAMP signaling pathway	56 (v172)	0.001	35 (total 154)	0.001
	Wnt signaling pathway	45 (total 141)	0.001	28 (total 130)	0.014
	TGF- β signaling pathway	33 (total 87)	0.002	19 (total 85)	0.036
	PI3K-Akt signaling pathway	78 (total 297)	0.005	50 (total 279)	0.025
	Calcium signaling pathway	44 (total 153)	0.007	31 (total 133)	0.005
TNF signaling pathway	33 (total 101)	0.032	24 (total 98)	0.007	

DE, differentially expressed genes.

by PGE₂ and downregulated by FGF2. Though many genes belonging to the cAMP signaling pathway were regulated in parallel by each treatment, the hallmark PKA-induced early gene *FOS* was repressed by FGF2, while *JUN*, whose protein product commonly binds FOS to form the AP-1 complex, was repressed by PGE₂. It is notable that both of these subunits of the archetypal AP-1 heterodimer — which has been shown to promote fibrosis (28, 29) — were reduced by either PGE₂ or FGF2. The WNT-associated genes *NFATC2*, *FZD1*, *FZD9*, and *WISP1* were upregulated by both treatments, whereas *WNT5A*, *WNT5B*, *WNT10B*, and *WNT11* were induced by PGE₂ and repressed by FGF2. The growth factors *FGF1*, *FGF5*, and *PDGFB* were all downregulated by PGE₂ and upregulated by FGF2, whereas *HGF*, shown to be antifibrotic (30) and deficient in IPF fibroblasts (31), was upregulated by PGE₂ but downregulated by FGF2. These results highlight many differences in gene regulation between PGE₂ and FGF2, even within mutually enriched pathways.

As discussed above, tissue contraction, ECM protein secretion, and apoptosis resistance are cardinal features of myofibroblasts. We therefore specifically interrogated the gene ontologies associated with these biologic processes. First, we found that PGE₂, and to a lesser extent FGF2, downregulated a number of important cytoskeletal, focal adhesion, and ECM-related genes (Figure 4A), including *ACTA2* and *ACTN1*. Both treatments reduced the expression of *MRTF1*, a transcription factor crucial for TGF- β -induced expression of α SMA in lung myofibroblasts (17). Neither treatment resulted in a significant change in *FN1* or *COL1A1* expression at the early time points at which sequencing analysis was performed, although each of these transcripts was reduced at later time points (Figure 1). Notably, PGE₂ suppressed the focal adhesion mediators *VASP*, *VLC*, *TLN1*, and *CTHRC1*, while FGF2 increased the expression of each. Though focal adhesion kinase (*PTK2*) was not significantly modulated by either treatment, the related gene *PTK2B*, which has similar biologic endpoints as *PTK2* (32), was markedly downregulated by both. Modulation of the extracellular matrix metalloproteases (MMPs) and their tissue inhibitors of metalloproteinase (TIMPs) was heterogeneous between treatments other than the mutual suppression of *MMP25* and *MMP28*. Finally, the pleiotropic growth factor *CTGF* was inversely regulated — decreased by PGE₂ and induced by FGF2.

Cellular differentiation and proliferation have long been considered to represent opposing or even mutually exclusive cellular programs (33). Indeed, it has been suggested that such a mechanism is integral to the ability of mitogens such as FGF2 to promote dedifferentiation (9). Predictably, myofibroblasts treated with FGF2 upregulated multiple cell cycle genes, including cyclins (*CCNB1*, *CCNB2*, *CCND1*, *CCND2*,

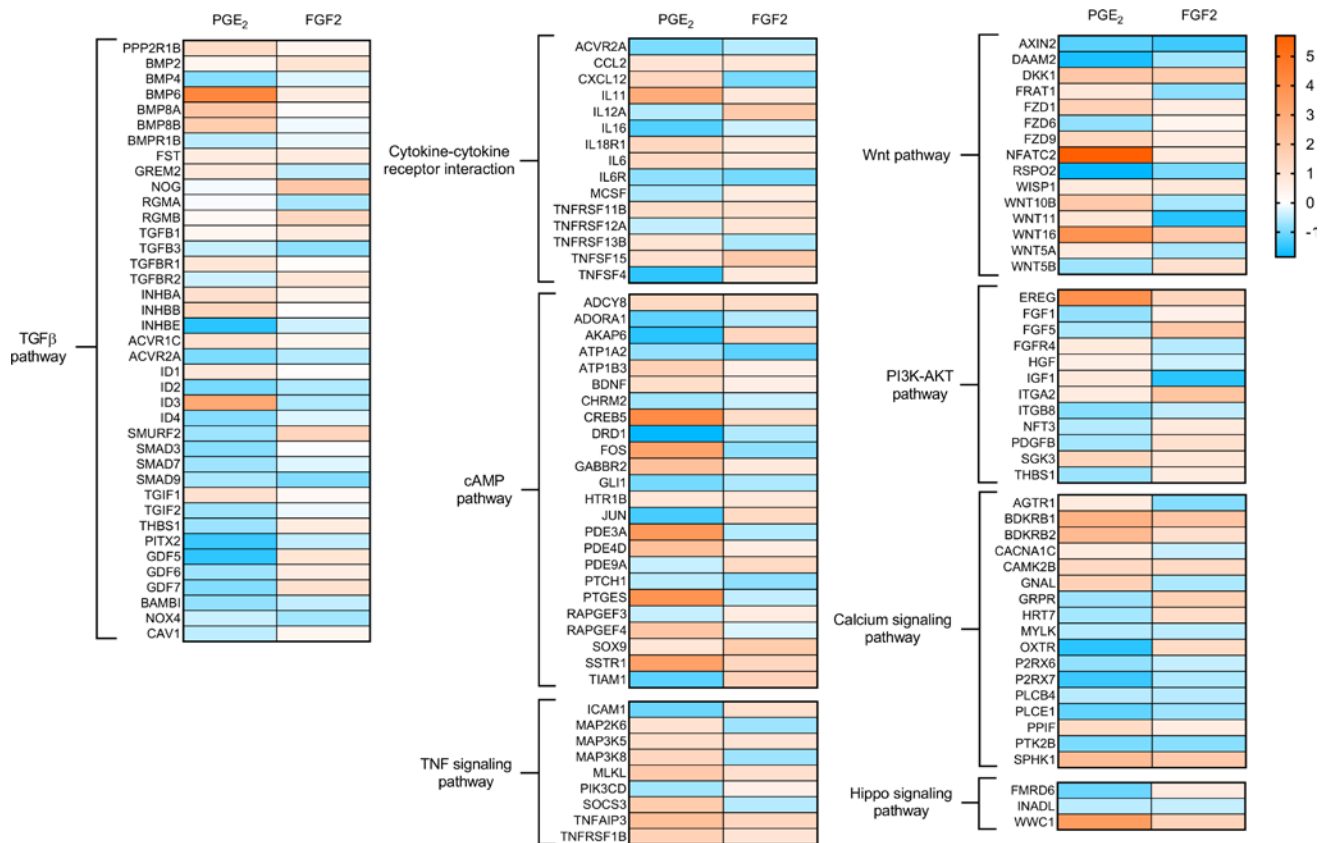


Figure 3. Regulation of genes from KEGG pathways enriched by both PGE₂ and FGF₂. Heatmap display of individual genes belonging to the specified pathways in myofibroblasts treated with PGE₂ or FGF₂ for 6 and 24 hours, respectively. Color scale depicts range of log₂ fold changes in gene expression.

and *CCNE2*), cyclin-dependent kinases (*CDK1*, *CDK2*, and *CDK7*), and *FOXM1* — a critical transcription factor in fibroblast proliferation (34) (Figure 4B). By contrast, PGE₂, which is well known to inhibit mesenchymal cell proliferation (33, 35, 36), exerted minimal effects on the expression of these genes and upregulated the cyclin-dependent kinase inhibitors *CDKN1C* and *CDKN2C*. Consistent with its proproliferative effects, FGF₂ increased prosurvival genes such as *BIRC5* and *MYC*, whereas PGE₂ increased the proapoptotic genes *APAF1* and *CASP9*. Finally, the profibrotic protein *SERPINE1*, well known to be overexpressed in IPF fibroblasts and reported to contribute to apoptosis resistance in myofibroblasts (37), was downregulated by PGE₂ but upregulated by FGF₂ (Figure 4B). These results indicate that PGE₂ and FGF₂ have largely opposing effects on genes involved in proliferation and apoptosis.

PGE₂ and FGF₂ modulate the expression of fibrosis-associated long noncoding RNAs and microRNAs in myofibroblasts. ncRNAs play significant roles in posttranscriptional regulation, as well as the determination and maintenance of cell phenotypes (38). Among these, a number of miRNAs exert pro- or antifibrotic effects by inhibiting translation and promoting RNA degradation (39, 40). Similarly, many long noncoding RNAs (lncRNAs) influence fibrosis through various mechanisms including miRNA “sponging” — preventing miRNA-mRNA interactions by competitive binding (41). Of the more than 8800 total lncRNAs identified, PGE₂ and FGF₂ modulated 811 and 261, respectively, with 100 shared among them (Figure 5, A and B). The top 25 regulated lncRNAs are listed in Supplemental Table 3. We curated a list of fibrosis-associated lncRNAs regulated by at least 1 of our treatments (Figure 5C). Both treatments downregulated *NEAT1* and *DNM3OS*, while PGE₂ reduced the profibrotic *PCAT1* and *PVT1*, and FGF₂ reduced *MALAT1*. The abundant lncRNAs *NEAT1* and *MALAT1* have been shown to contribute to organ fibrosis and to sponge numerous miRNAs (42, 43), while *DNM3OS* has been reported to promote the expression of the profibrotic miR-214-3p and miR-199a-3p/5p in human lung fibroblasts (44). PGE₂ also increased the antifibrotic lncRNA *FENDRR*, which sponges miR-214-3p and is known to be reduced in IPF fibroblasts (45).

Though over 350 miRNAs were detected under each treatment condition, PGE₂ only significantly modulated 3 miRNAs while FGF₂ regulated 23 (Figure 5, D and E, Supplemental Table 4). Both PGE₂

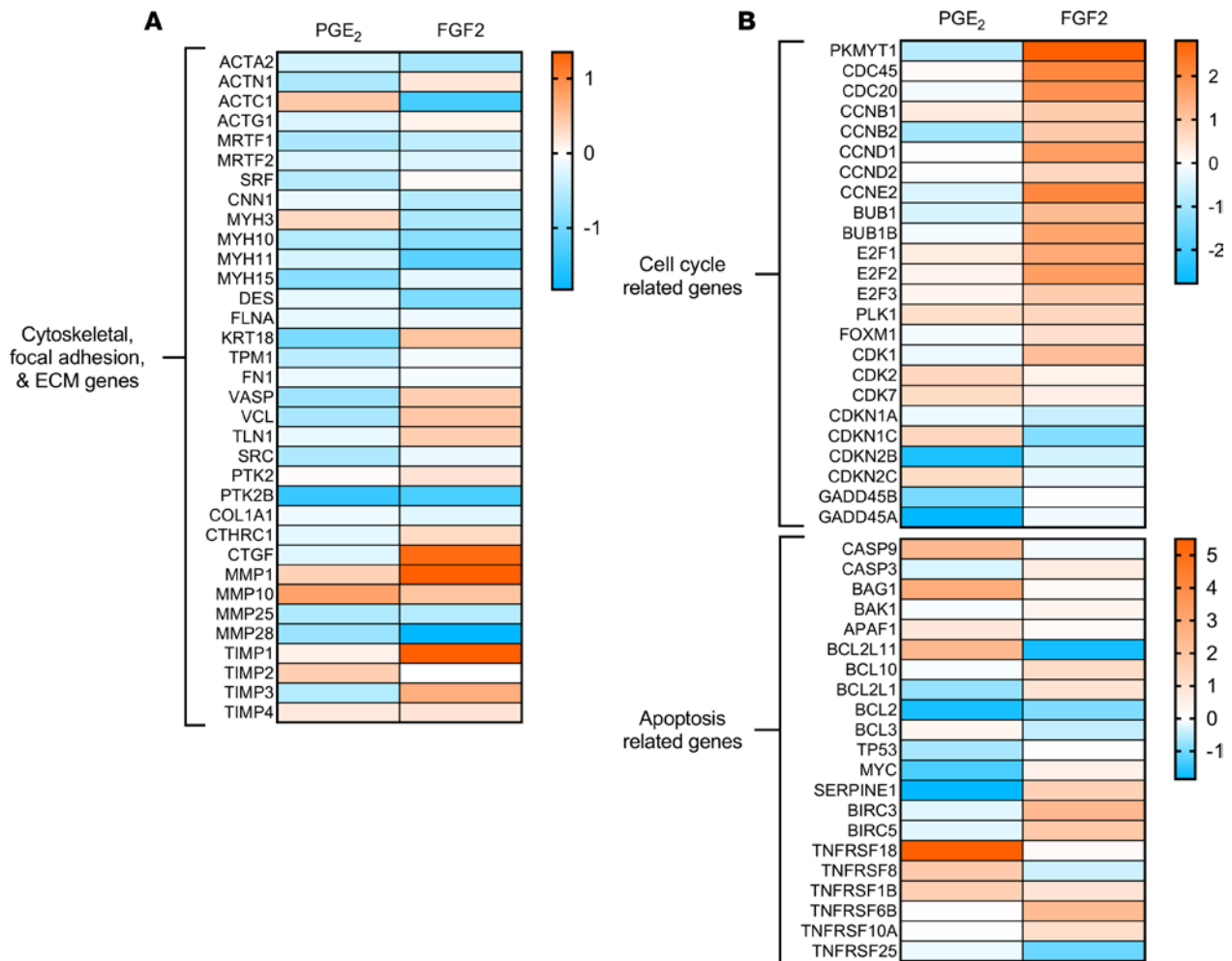


Figure 4. Gene ontology characteristics of myfibroblasts following treatment with PGE₂ or FGF2. (A and B) Heatmap display of cytoskeletal, ECM-related, and focal adhesion (A) and cell cycle and apoptosis genes (B) in PGE₂- and FGF2-treated myfibroblasts compared with 6- and 24-hour time-matched controls. Color scale depicts range of log₂ fold changes in gene expression. ECM, extracellular matrix.

and FGF2 increased expression of miR-543, which has been shown to inhibit TGF- β activation and gene expression in rat cardiac fibroblasts (46). miR-335-3p, an antiproliferative and proapoptotic miRNA with antifibrotic properties in gingival fibroblasts (47, 48), was upregulated by PGE₂ and repressed by FGF2. The top PGE₂-upregulated miRNA, miR-129-5p, exhibits antifibrotic actions in dermal fibroblasts by targeting *COL1A1* (49). Furthermore, FGF2 upregulated the antifibrotic miR-29b-3p/5p, miR-152-5p, and let-7a-3p (5, 50, 51), while downregulating the profibrotic miR-145-3p (52). Other profibrotic- and antifibrotic-associated miRNAs — including miR-21 (53) and miR-27a-3p/miR-27b-3p (54) — were detected in high abundance in our analysis but were not differentially regulated by either treatment (Supplemental Table 5). As discussed above, miRNA activity can be regulated through RNA sponging without changes in miRNA expression (38, 55). Indeed, multiple differentially expressed lncRNAs in our analysis have been shown to affect the function of a number of fibrosis-associated miRNAs that were not, themselves, differentially regulated in our study (Table 2). These data indicate a possible role for ncRNAs in PGE₂- and FGF2-mediated dedifferentiation of myfibroblasts.

Myfibroblasts treated with PGE₂ and FGF2 separately or in combination produce distinct cellular morphologies and fibrosis-associated gene expression patterns. To complement their distinct transcriptomic effects, we sought to examine the influence of PGE₂ and FGF2 on myfibroblast morphology. Furthermore, we wished to determine the net effect of combining these 2 effector molecules — a closer approximation of the in vivo conditions in which they would be expected to coexist — on cell morphology, loss of stress fibers, and the expression of various fibrosis-associated genes. Undifferentiated fibroblasts stained with the membrane dye

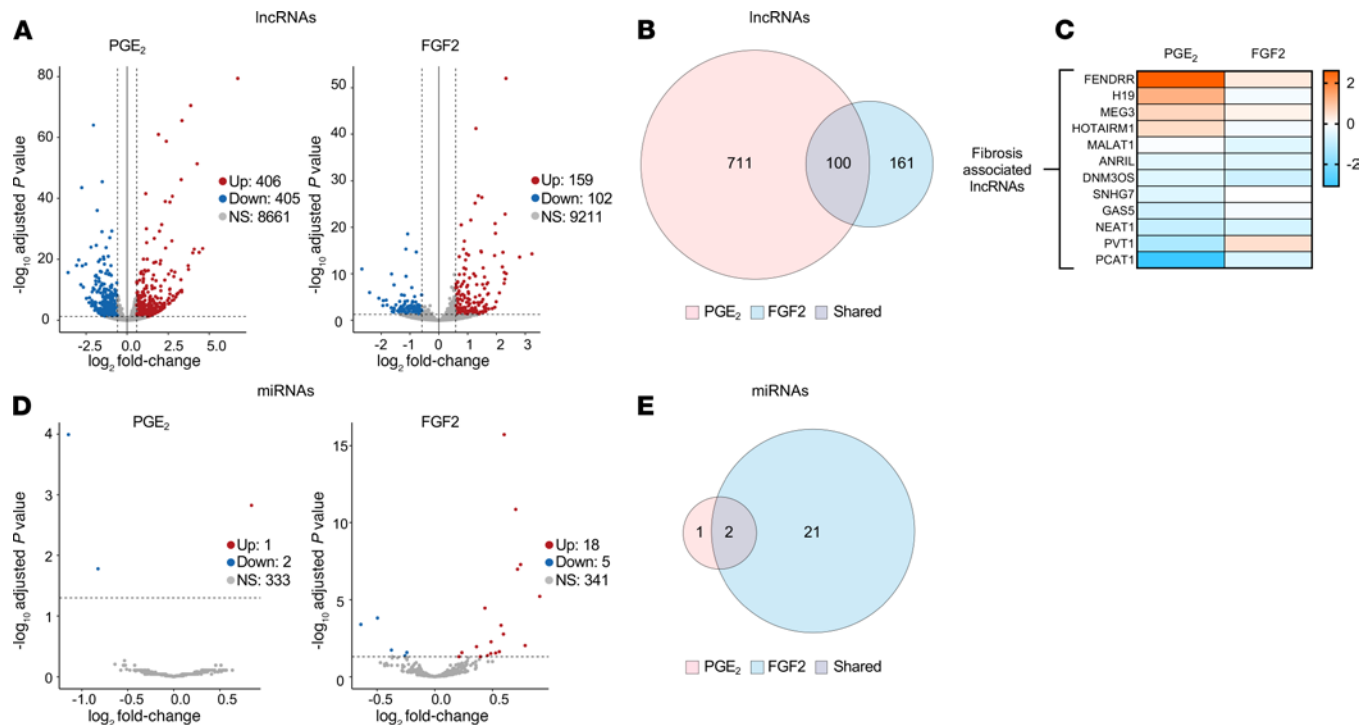


Figure 5. PGE₂ and FGF2 modulate the expression of fibrosis-associated long noncoding RNAs and miRNAs in myfibroblasts. (A and D) Volcano plots representing differential lncRNA expression (A) miRNA expression (D) by log₂ fold change (x axis) and adjusted *P* value (y axis) of total RNA transcripts in PGE₂- and FGF2-treated myfibroblasts compared with time-matched controls. Threshold for lncRNAs set by log₂ fold change -0.5 to 0.5 and adjusted *P* < 0.05 . Threshold for miRNAs set by adjusted *P* < 0.05 only. (B and E) Venn diagrams depicting the number of differentially expressed lncRNAs (B) and miRNAs (E) exclusively by PGE₂ (red), exclusively by FGF2 (blue), and by both mediators (gray). (C) Heatmap display of fibrosis-associated lncRNAs differentially regulated by PGE₂ and/or FGF2. Color scale depicts range of log₂ fold changes in gene expression.

PKH26 appeared spindle shaped and elongated, in stark contrast to the larger, cuboidal, and stellate-shaped myfibroblasts (Figure 6A). Compared with untreated myfibroblasts, those subsequently exposed to PGE₂ appeared smaller and thinner, and they displayed fewer cytoplasmic projections. FGF2-treated myfibroblasts lost their stellate shape, appearing thin and elongated, similar to native fibroblasts. The combination of PGE₂ and FGF2 produced a small, more rounded cell, distinct from the transitional cell morphology produced by either treatment alone. We assessed the kinetics of *ACTA2* in response to each treatment, as well as their combination (Figure 6B). Combined treatment displayed an effect that was statistically greater than that with either treatment alone at 24, 48, and 72 hours. Interestingly, though PGE₂ treatment resulted in a more rapid reduction in *ACTA2* through 24 hours, its effects plateaued at 48 hours, whereas FGF2 progressively reduced *ACTA2* through 72 hours. Combined treatment also reduced α SMA protein and its organization into stress fibers (Figure 6C) to an extent apparently greater than did either treatment alone (Figure 1B). We next performed quantitative PCR (qPCR) on selected fibrotic genes to further evaluate the effect of combined treatment on each (Figure 6D). As displayed in Figure 6B, combined treatment with PGE₂ and FGF2 reduced *ACTA2* at 24 hours to a greater extent than either treatment alone. There was a trend toward an additive reduction in *COL1A1*. *FNI* reduction in response to PGE₂ and FGF2 appeared comparable in magnitude to PGE₂ alone. Though the profibrotic growth factor *CTGF* and focal adhesion regulator *VASP* were each downregulated by PGE₂ and upregulated by FGF2, combination treatment resulted in reduced expression of each transcript. Expression of *NOX4* was reduced in PGE₂- and FGF2-treated myfibroblasts, though combination treatment did not yield any further reduction.

PGE₂ and FGF2 have opposite effects on myfibroblast proliferation and apoptosis. Our transcriptomic analysis predicted that treatment of myfibroblasts with PGE₂ would inhibit their capacity for proliferation and reestablish apoptosis sensitivity, while treatment with FGF2 would promote proliferation and maintain apoptosis resistance. We tested these predictions by directly assaying proliferation capacity and apoptosis sensitivity in myfibroblasts treated with PGE₂ and/or FGF2 as compared with untreated controls. First, we assessed the expression of cell cycle genes (Figure 7A, top panel) and apoptosis genes (Figure 7A, bottom

Table 2. Fibrotic effects and selected miRNA interactions of lncRNAs regulated by PGE₂ or FGF2

lncRNA	Effect of PGE ₂	Effect of FGF2	Effect on Fibrosis	miR interactions	Reference
PCAT1	↓↓↓	↓	Profibrotic	Sponges miR-145	(83, 84)
PVT1	↓↓	↑	Profibrotic	Sponges miR-214-3p	(85, 86)
NEAT1	↓	↓	Profibrotic	Sponges miR 27a	(42, 87)
DNM3OS	↓	↓	Profibrotic	induces miR-214-3p, -199-3p/5p	(44)
MALAT1	↔	↓	Profibrotic	Sponges miR-199a-3p, -125b	(43, 88, 89)
H19	↑↑	↔	Profibrotic	Sponges let-7 family	(86)
FENDRR	↑↑↑	↔	Anti-fibrotic	Sponges miR-214	(45)
MEG3	↑	↔	Anti-fibrotic	Sponges miR-21-5p, -29	(86, 90, 91)
GAS5	↓	↓	Anti-fibrotic	Sponges miR-21	(92)

Arrows represent the following log₂ fold changes: ↑ 0.5 to 1.0; ↑↑ 1.0 to 2.0; ↑↑↑ >2.0; ↓ -0.5 to -1.0; ↓↓ -1.0 to -2.0; ↓↓↓ < -2.0; ↔ NS.

panel) in myofibroblasts exposed to each treatment alone and in combination. *CCNB2*, *CCND1*, and *FOXM1* were upregulated by FGF2, consistent with our RNA-seq data. Importantly, though PGE₂ did not significantly modulate these genes, it negated their upregulation by FGF2. Conversely, the expression of the cyclin-dependent kinase inhibitor *CKDNIC* was greatly and uniquely increased by PGE₂, an increase not fully abrogated by addition of FGF2. The antiapoptotic genes *BIRC5* and *SERPINE1* were each uniquely upregulated by FGF2, but such increases were partially or completely abrogated by the addition of PGE₂, while *MYC* was downregulated by PGE₂ in the presence or absence of FGF2. The proapoptotic gene *CASP9*, which leads to activation of *CASP3* (56), was upregulated by PGE₂ and downregulated by FGF2, and it remained slightly upregulated with combined treatment. Taken together, these data demonstrate that PGE₂ and FGF2 have opposing effects on myofibroblast genes associated with proliferation and apoptosis.

We next determined if these transcriptomic differences were associated with functional differences in myofibroblast proliferation and apoptosis. Consistent with the effect of each treatment on cell cycle genes, FGF2 increased the proliferation of established myofibroblasts, whereas PGE₂ had no effect relative to untreated myofibroblasts but abolished the proliferative effects of FGF2 (Figure 7B). To assess the apoptosis sensitivity of myofibroblasts undergoing dedifferentiation, we treated cells with PGE₂ and/or FGF2 for 5 days prior to treatment with an anti-Fas activating antibody; apoptosis was assessed by Western blot detection of cleaved/total *CASP3* and *PARP* within cell lysates (Figure 7C). As expected, the levels of cleaved *CASP3* and *PARP* did not increase in response to Fas activation of untreated myofibroblasts, highlighting their intrinsic resistance to apoptosis. In contrast, myofibroblasts dedifferentiated with PGE₂ displayed significantly higher levels of cleaved *CASP3* and *PARP* after exposure to anti-Fas activating antibody relative to untreated myofibroblasts. Such an effect was not seen in myofibroblasts dedifferentiated with FGF2, but it was preserved in myofibroblasts dedifferentiated with both agents together. To assess whether restoration of apoptosis sensitivity in myofibroblasts elicited by PGE₂ depends on prior dedifferentiation, we performed immunofluorescence microscopy for annexin V and α SMA in PGE₂-treated myofibroblasts and untreated myofibroblast controls subsequently exposed to anti-Fas for 4 hours (Supplemental Figure 3). Notably, we found a small proportion of PGE₂-treated myofibroblasts that retained their stress fibers, suggesting underlying fibroblast heterogeneity. PGE₂-treated myofibroblasts undergoing apoptosis — defined by annexin V staining — were almost exclusively limited to those lacking α SMA stress fibers. Untreated myofibroblasts did not exhibit annexin V staining, further confirming their resistance to apoptosis.

Lung fibroblasts from an in vivo model of fibrosis resolution exhibit similar gene signatures as those determined in myofibroblasts dedifferentiated in vitro. The RNA-seq data presented thus far were derived from in vitro treatment of myofibroblasts with individual mediators. To evaluate the relevance of these findings in a less reductionist and in vivo model of fibrosis resolution, we compared the transcriptome of freshly isolated lung fibroblasts from young mice with that of lung fibroblasts isolated from aged mice following bleomycin challenge. It has been established that, in contrast to aged mice, young mice subjected to bleomycin-induced pulmonary fibrosis can undergo spontaneous resolution — in which fibroblasts reduce collagen secretion and lose their α SMA stress fibers (57–59). To characterize their global transcriptome, RNA-seq was performed on FAC-sorted fibroblasts isolated from the lungs of young mice (2 months) and aged mice (18

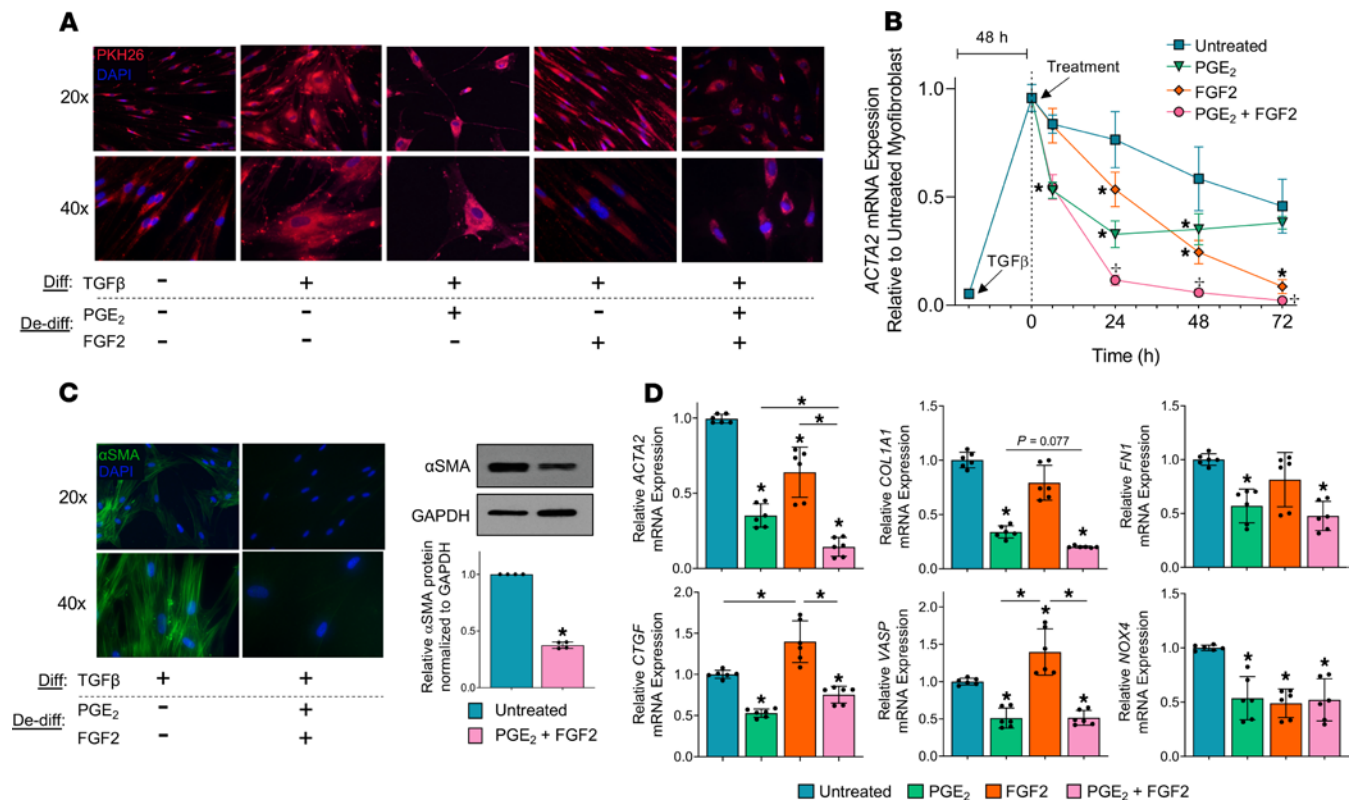


Figure 6. Myfibroblasts treated with PGE₂ and FGF2 separately or in combination produce distinct cellular morphologies and fibrosis-associated gene expression patterns. CCL210 fibroblasts were differentiated to myfibroblasts with TGF-β (2 ng/mL) and treated with PGE₂ (1 μM), FGF2 (50 ng/mL), or both. (A) Cells were stained with the membrane dye PKH26 (2 μM) and examined by fluorescence microscopy 5 days after treatment. (B) Kinetics of ACTA2 in untreated, PGE₂-, FGF2-, and PGE₂ + FGF2-treated myfibroblasts. Fibroblasts were treated with TGF-β for 48 hours, followed by treatment and harvesting for mRNA at the indicated time points. (C) Immunofluorescence microscopy and representative Western blot for αSMA in untreated and PGE₂ + FGF2-treated myfibroblasts evaluated at 5 days. The histogram depicts mean densitometry values. (D) qPCR analysis of the fibrosis-associated genes ACTA2, COL1A1, FN1, CTGF, VASP, and NOX4 after 24 hours of PGE₂ ± FGF2 compared with untreated myfibroblast control. Relative fold changes of indicated genes measured by qPCR are normalized to GAPDH. Data are presented as mean ± SEM; data points represent replicate samples from 3 experiments. Lines indicate conditions being compared. *Statistical significance compared with untreated myfibroblast; *Statistical significance compared with untreated, PGE₂-, and FGF2-treated myfibroblasts. *P < 0.05 and *P < 0.05. Performed 2-way ANOVA for B, paired 2-tailed t test for C, and 1-way ANOVA for D. Diff, differentiation; De-diff, dedifferentiation.

months) during the early phase of fibrosis resolution (30 days after bleomycin) (Figure 8A). A comprehensive analysis of these data is described in a separate manuscript currently in preparation; herein, we present limited data from this dataset relevant to cell cycle, apoptosis, and focal adhesion genes found to be significantly modulated by either PGE₂ or FGF2 treatment of myfibroblasts in vitro (Figure 4, A and B). Gene expression changes in fibroblasts isolated from young lungs undergoing fibrosis resolution were expressed relative to those of fibroblasts isolated from aged mouse lungs with nonresolving fibrosis (Figure 8B).

Lung fibroblasts sorted from mouse lungs undergoing fibrosis resolution expressed lower levels of proliferation genes, including *Ccnb1*, *Ccnb2*, *Cnd1*, *Cnel1*, *Cdk1*, and *Foxm1*. Conversely, the antiproliferative *Cdkn1c* was upregulated. Five of the eighteen significantly modulated cell cycle genes in fibroblasts from mice with resolving fibrosis were regulated in parallel to PGE₂-treated human myfibroblasts, while just 1 gene was regulated in parallel to FGF2-treated myfibroblasts. Notably, 15 of these 18 cell cycle genes were regulated oppositely to that of FGF2-treated myfibroblasts in vitro, whereas only 3 genes were regulated opposite to PGE₂-treated myfibroblasts. The proapoptotic gene *Casp9* was upregulated in fibroblasts from mice with resolving fibrosis, and the prosurvival genes *Birc5*, *Birc3*, and *Serpine1* were all downregulated. Of the 10 apoptosis-associated genes significantly modulated in young lung fibroblasts, 3 were regulated in parallel with PGE₂-treated versus 1 in FGF2-treated myfibroblasts. Interestingly, the apoptosis-associated genes *Myc*, *Bcl2l1*, *Bcl2l11*, and *Tnfrsf8* — which were regulated oppositely by PGE₂ and FGF2 in vitro — showed no significant differences between fibroblasts isolated from mice with resolving and nonresolving fibrosis, suggesting an in vivo level of expression reflecting the arithmetic sum of changes elicited individually by PGE₂ and FGF2 in vitro. Eight of 10 significantly modulated focal adhesion genes were also

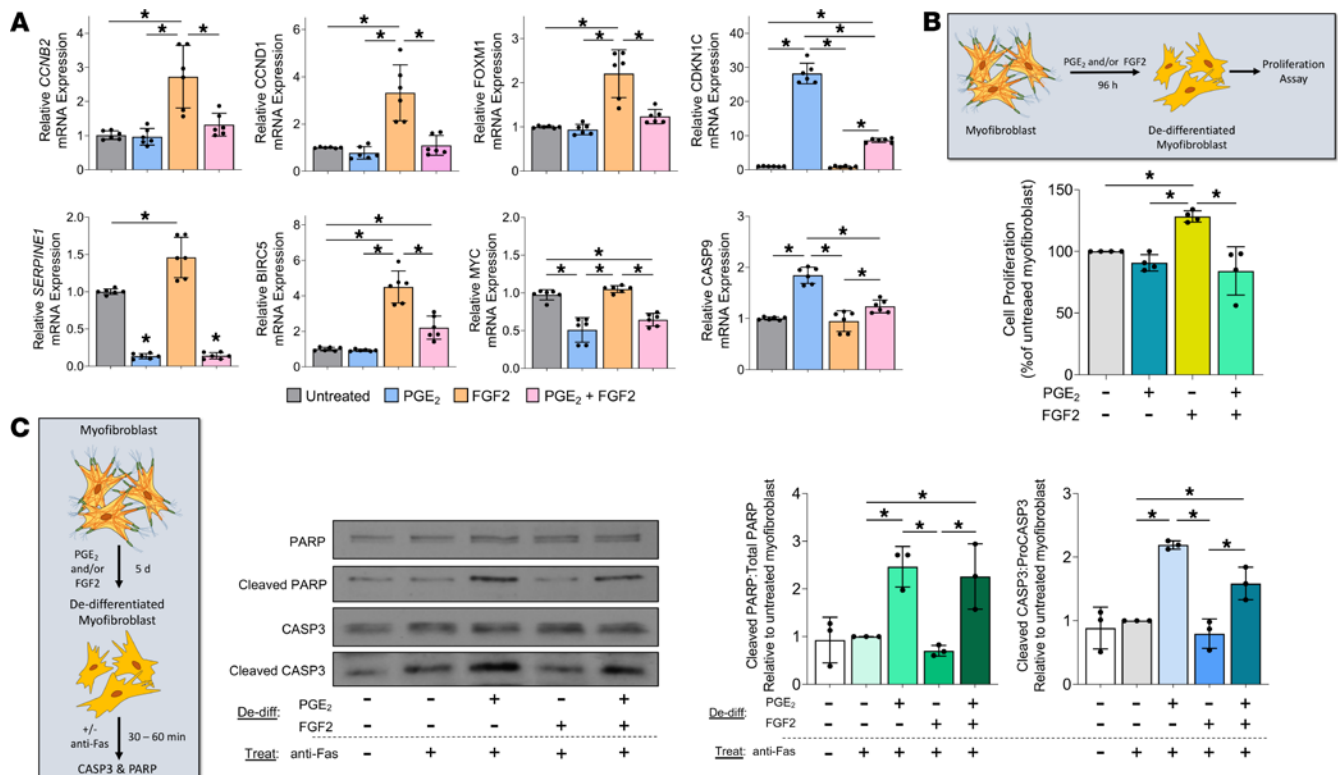


Figure 7. PGE₂ and FGF2 have opposite effects on myfibroblast proliferation and apoptosis. (A) CCL210 myfibroblasts were treated with PGE₂, FGF2, or PGE₂ + FGF2 for 24–72 hours. qPCR analysis of the proliferation gene *FOXM1* was performed at 48 hours, while *CCNB2*, *CCND1*, and *CDKN1C* were assessed at 72 hours (top panel). qPCR analysis of the antiapoptotic gene *SERPINE1* was performed at 24 hours, while *BIRC5* and *MYC* were assessed at 48 hours; the proapoptotic gene *CASP9* was assessed at 72 hours. (B) Proliferation was assessed 96 hours following treatment with PGE₂ and/or FGF2 by CyQUANT Cell Proliferation Assay. (C) Apoptosis sensitivity was assessed by measuring total and cleaved CASP3 and PARP by Western blot analysis in myfibroblasts 5 days following addition of PGE₂ and/or FGF2, followed by treatment with the death receptor ligand anti-Fas. CASP3 was measured 30 minutes and PARP 1 hour following anti-Fas treatment. Densitometry represents ratio of cleaved products to total protein. Relative fold changes of indicated genes measured by qPCR are normalized to *GAPDH*. Data are presented as mean ± SEM. Data points represent replicate samples from 3 (A and C) or 4 (B) experiments. Lines indicate conditions being compared. **P* < 0.05, compared with untreated myfibroblast; 1-way ANOVA. De-diff, dedifferentiation.

downregulated in parallel with the PGE₂-treated myfibroblasts. Among these were *Vasp* — a phosphoprotein involved in actin assembly and SRF activity (60) — and *Cthrc1*, which is a marker of tissue fibrosis (61). In contrast, FGF2-treated myfibroblasts showed opposite regulation of *Vasp*, *Vcl*, *Tln*, and *Cthrc1*. *Col1a1* and *PTK2B* were the only genes assessed among these pathways that were concordantly regulated by PGE₂ and FGF2 treatment of myfibroblasts in vitro as well as in fibroblasts from mice during fibrosis resolution.

Discussion

Myfibroblasts are critical effector cells that orchestrate, maintain, and propagate lung scarring in IPF and other fibrotic disorders (62). Whereas inhibiting the fibroblast to myfibroblast transition has the potential to prevent fibrogenesis in response to a recognized injury and to arrest progression of an established fibrotic process, it is unlikely to be sufficient to promote its resolution. By contrast, promoting myfibroblast clearance has the potential to do so. Since elimination of myfibroblasts in fibrotic diseases is limited by their resistance to apoptosis, dedifferentiation provides a potential route to restore apoptosis sensitivity and, thus, facilitate myfibroblast removal. Indeed, myfibroblast dedifferentiation has been reported in response to a variety of effector molecules, including mitogens such as serum and FGFs (13, 14), lipid mediators PGE₂ and PGI₂ (10, 63), statins (64), siRNA knockdown of the transcription factors MyoD (33) and FOXM1 (34), and the bromodomain inhibitor JQ1 (65). Whether dedifferentiation with these diverse classes of effector molecules yields common or divergent transitional cell phenotypes has not previously been explored. Here, we compared the operative signaling mechanisms, as well as the transcriptomic, morphologic, and functional characteristics, of myfibroblasts treated with the endogenous soluble mediators PGE₂ and FGF2.

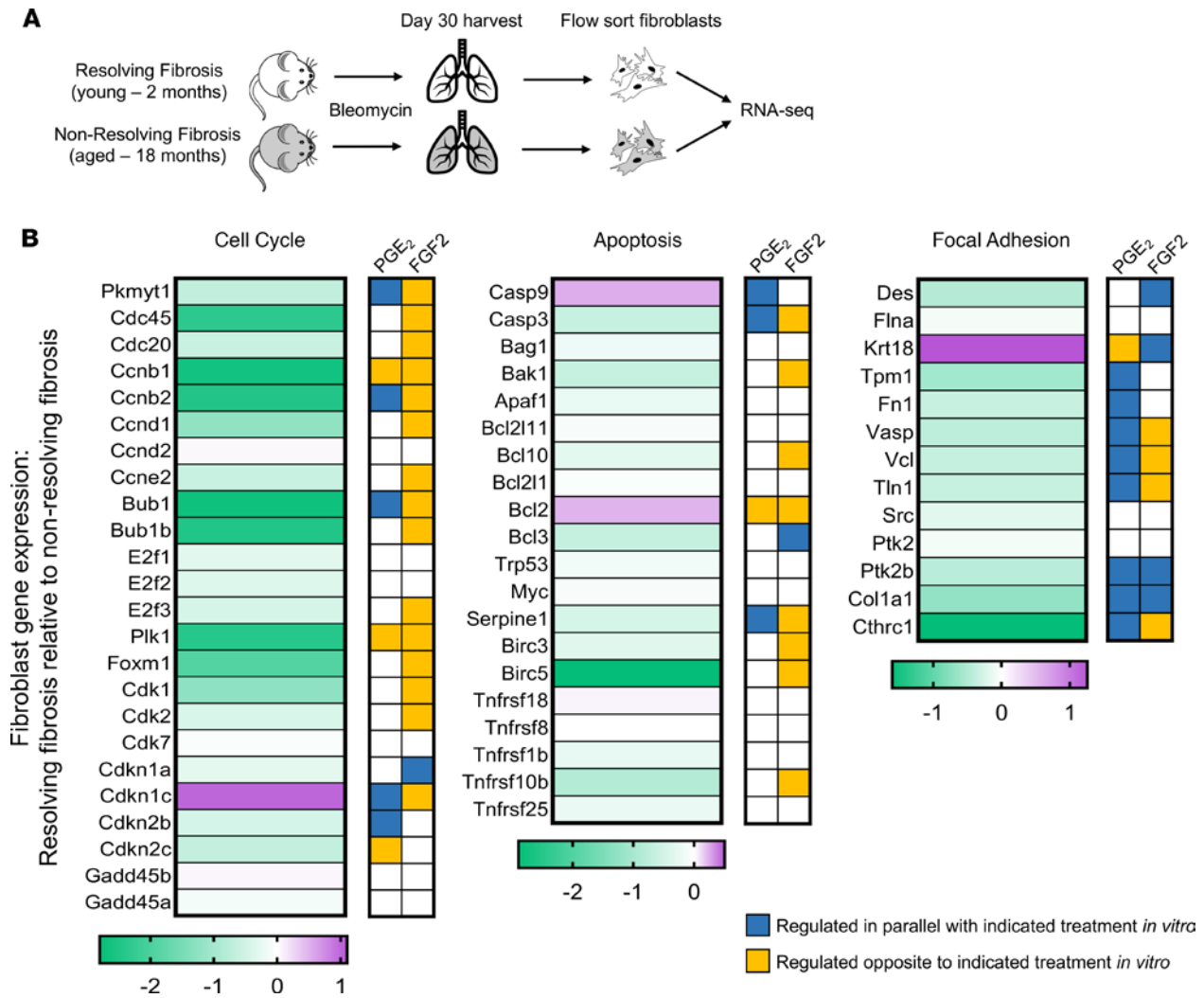


Figure 8. Lung fibroblasts from an in vivo model of fibrosis resolution exhibit similar gene signatures as those determined in myofibroblasts dedifferentiated in vitro. (A) Experimental scheme for bleomycin-induced pulmonary fibrosis in Col1 α 1-GFP⁺ mice with resolving fibrosis (young) and nonresolving fibrosis (aged); mice were sacrificed on day 30, and fibroblasts were flow sorted from lungs and submitted for RNA-seq. (B) Heatmap display of gene expression in mice with resolving fibrosis (compared with the expression in mice with nonresolving fibrosis). Color scale depicts range of log₂ fold changes in gene expression. *Tnfrsf10b* is the mouse homolog of human *TNFRSF10A*. Gene expression patterns regulated in parallel (blue) or opposite (yellow) to those exhibited with in vitro treatments of human myofibroblasts are indicated in color-filled boxes to the right of the heatmaps.

Our results confirm that PGE₂ and FGF2 are both capable of dedifferentiating human lung myofibroblasts by downregulating α SMA and eradicating stress fibers (Figure 1, B and C). However, they accomplish this via distinct signaling pathways and with different kinetics (Figure 1, B, D, and E; and Figure 6B). Globally, PGE₂ modulated nearly double the number of protein-coding genes and nearly triple the number of ncRNAs, and it induced greater log-fold changes among top-regulated genes than did FGF2 (Figure 2B, Figure 5A, and Supplemental Table 1). Moreover, each mediator produced a unique transitional cell phenotype characterized by distinctive gene programs, morphology, proliferative capacities, and sensitivity to apoptosis (Figures 3–7).

It is now recognized that myofibroblasts have multiple potential fates (8, 66–68). While myofibroblast senescence favors their persistence and, thus, progression of fibrotic disease (9), we demonstrate herein that deactivation and proliferation represent 2 distinct paths by which myofibroblasts can dedifferentiate. As in prior studies establishing that PGE₂ inhibits many critical functions of fibroblasts — including proliferation, differentiation, contractility, and focal adhesion (17, 19, 69) — we show here that PGE₂ also deactivates these same processes in myofibroblasts (Figures 1, 3, 4, and 7). By contrast, the potent fibroblast mitogen FGF2 (34) stimulates proliferation in myofibroblasts (Figure 4B and Figure 7, A and B). These comparative data suggest that, while FGF2 dedifferentiates lung myofibroblasts primarily by promoting their proliferation, PGE₂

accomplishes this via a much more global form of cellular deactivation. A major and functionally important consequence of these divergent mechanisms of dedifferentiation is that transitional cells resulting from PGE₂ exposure are more, while those resulting from FGF2 exposure are less, susceptible to apoptosis (Figure 7C).

It is likely that in order to undergo cell division, dedifferentiating myofibroblasts must restructure their cytoskeletal network and matrix interactions. Indeed, FGF2 downregulated α SMA, stress fibers, and collagen I in established myofibroblasts via activation of the MEK/ERK pathway (Figure 1, B, C, and E), which has also been previously shown to mediate proliferation in myofibroblasts (33). Morphologically, FGF2-treated myofibroblasts elongate and lose their stellate shape, resembling native fibroblasts (Figure 6A). Overexpression of FGF2 has similarly been reported to inhibit myofibroblast differentiation in vitro and pulmonary fibrosis in vivo (14). In contrast to the mechanisms of action of FGF2, PGE₂ dedifferentiates myofibroblasts (Figure 1D) while concomitantly inhibiting their proliferation (Figure 7B), effects likely to be mediated through cAMP/Epac (35), rather than ERK (Supplemental Figure 1C). In addition to our current findings and our previously published microarray data (12) demonstrating that PGE₂ remodels the global transcriptome of established myofibroblasts, the importance of cAMP signaling in this regard is further validated by recent parallel findings with a PGI₂ analog acting via its G_s-coupled receptor (63).

In addition to modulating mRNA expression, PGE₂ and FGF2 differentially regulated multiple lncRNAs and miRNAs in lung myofibroblasts (Figure 5). Several ncRNAs modulated in our study have been reported to influence myofibroblast function and fibrotic outcomes. Importantly, many antifibrotic miRNAs that were not significantly modulated by either treatment do, in fact, interact with lncRNAs modulated by PGE₂ and/or FGF2 (Table 2). The ncRNAs encompass a large family of pleiotropic posttranscriptional regulators that control the expression of gene programs through complex lncRNA-miRNA-mRNA interactions (70, 71). We, therefore, speculate that lncRNAs and miRNAs may be important for the effects of both PGE₂ and FGF2 in myofibroblasts. Their coordinated actions remain to be more comprehensively defined, and these data provide a blueprint for doing so in future studies.

Since myofibroblast dedifferentiation elicited by PGE₂ and FGF2 — expected constituents of an injured/fibrotic lung (72, 73) — proceeded via distinct signaling mechanisms and gene expression programs, we assessed their individual and combined effects on *ACTA2* kinetics, myofibroblast morphology, dedifferentiation, proliferation, and apoptosis sensitivity. Indeed, myofibroblasts treated with both mediators displayed an additive reduction in α SMA mRNA, protein, and stress fibers (Figure 6, B and C), while also exhibiting a morphology distinct from that of either treatment alone (Figure 6A). The effects of combined versus individual treatment on specific fibrosis-associated genes ranged from additive inhibition (*ACTA2*) to no additive effect (*NOX4*) to a dominant effect of PGE₂ (*CTGF* and *VASP*) (Figure 6D). Moreover, PGE₂ functioned to negate the proliferative and antiapoptotic effects of FGF2 (Figure 7).

The inherently reductionist nature of our in vitro studies limits the conclusions that can be drawn. In an effort to more broadly contextualize such findings, we compared our data to selected transcriptomic differences in lung fibroblasts obtained during an in vivo model of fibrosis resolution. We acknowledge that the in vivo and in vitro models differed with respect to the species utilized and the timing of analysis. Additionally, the in vivo data lack a time point corresponding to peak fibrosis in the young mice, and instead, we compared the data from mice undergoing fibrosis resolution with those from mice with nonresolving fibrosis. Despite these limitations, substantial parallels in the gene signatures of the mesenchymal cells from the 2 models were apparent and intriguing. Fibroblasts from mice undergoing the early stages of fibrosis resolution exhibited an antiproliferative, proapoptotic, and antiadhesion gene signature, which resembled that seen in PGE₂-treated and PGE₂ + FGF2-treated myofibroblasts (Figure 4, A and B, and Figure 7A). It is understood that mesenchymal cell responses to PGE₂ and/or FGF2 in culture and during fibrosis resolution in vivo may involve the differential behaviors of phenotypically distinct fibroblast subpopulations (74, 75). Moreover, the exclusive use of bulk RNA-seq analysis in both models represents an additional limitation of our study, and single cell approaches — as well as flow sorting of isolated fibroblast subpopulations (76) — will be necessary in the future to assess the cellular heterogeneity of mesenchymal responses during dedifferentiation and fibrosis resolution. Additionally, we acknowledge the importance of confirming these findings in human IPF cells.

Although our study was primarily undertaken to gain a better understanding of the process of myofibroblast dedifferentiation, its potential therapeutic ramifications for fibrotic diseases cannot be ignored. Indeed, inhibition of the PGE₂-degrading enzyme 15-PGDH has recently been shown to attenuate lung fibrosis in vivo and to reduce collagen levels in lung slices from IPF patients (77). Our results therefore suggest that, in principal, activation of the cAMP/PKA pathway and MEK/ERK have the potential to lead

to fibrosis resolution. Notably, this raises the possibility that, by blocking FGFR signaling, the antifibrotic drug nintedanib might promote and maintain myofibroblasts, which in turn may limit its therapeutic efficacy. Increasing cAMP can be achieved in a variety of ways pharmacologically, including treatment with the FDA-approved phosphodiesterase inhibitor roflumilast. Pharmacologic strategies to activate ERK are currently under investigation for use as therapeutics in cancer (78, 79). Combined activation of these pathways represents an attractive therapeutic strategy due to their additive effects on myofibroblast dedifferentiation with restoration of apoptosis sensitivity. The potential of these approaches requires further investigation.

In this study, we have compared — for the first time to our knowledge — the transcriptomic, morphologic, and functional changes in PGE₂- and FGF2-dedifferentiated lung myofibroblasts. Although PGE₂- and FGF2-treated myofibroblasts differed in their abilities to proliferate and undergo apoptosis, combined treatment resulted in an antiproliferative/proapoptotic phenotype and an additive effect on dedifferentiation. The cell cycle, apoptosis, and focal adhesion gene signatures exhibited by cells from mice undergoing fibrosis resolution more closely resembled those elicited by myofibroblast treatment with PGE₂ than with FGF2, but they most closely paralleled the effects of combined PGE₂ + FGF2 treatment in vitro. Mechanistically, PGE₂ induced dedifferentiation via cAMP-mediated deactivation of myofibroblasts, whereas FGF2 utilized MEK/ERK to prompt dedifferentiation through myofibroblast proliferation. As neither of the current therapies for IPF exploit cAMP signaling, and as nintedanib antagonizes ERK, our results highlight additional pathways and gene programs that hold promise and warrant further investigation in the development of novel therapeutics for this and other fibrotic diseases.

Methods

Cell culture. CCL210 normal adult human lung fibroblasts were obtained from the American Type Culture Collection. Cell culture was performed in low glucose DMEM (Invitrogen) supplemented with 10% FBS (Hyclone), 100 units/mL penicillin, and 100 µg/mL streptomycin (both from Invitrogen). Cells were then serum starved in FBS-free DMEM overnight, and differentiation to myofibroblasts was induced by treatment with TGF-β for 48 hours. TGF-β-elicited myofibroblasts were then treated for specified time points as described followed by harvesting (10).

Reagents. Unless otherwise specified, pharmacologic agents were reconstituted in DMSO as stock solutions and stored at -80°C with working concentrations indicated in parentheses. Recombinant human TGF-β (2 ng/mL) and FGF2 (50 ng/mL) were purchased from R&D and stored in filter-sterilized 1% BSA at -20°C. Inhibitors of the MAPKs MEK/ERK (PD98059, 20 µM; U0126, 20 µM) and p38 (SB203580, 20 mM) were purchased from Cayman Chemicals and stored at -20°C. PGE₂ (1 µM) purged with nitrogen gas, the E-prostanoid 2 agonist butaprost (500 nM), the direct adenylyl cyclase activator forskolin (500 nM), the JNK inhibitor SP600125 (20 mM), and the AKT-1, -2, -3 inhibitor Triciribine (20 mM) were purchased from Cayman Chemicals. The PKA-selective cAMP agonist 6-BNZ cAMP (2 mM) and the Epac-selective agonist 8-pCPT cAMP (2 mM) were purchased from BioLog and reconstituted in sterile water. Fast and Power SYBR Green Master Mix and StepOne real-time PCR system were procured from Applied Biosystems. An αSMA primary antibody conjugated to a FITC-conjugated secondary antibody (F3777, Sigma-Aldrich), polyclonal annexin V antibody (PA5-57231, Thermo Fisher Scientific), PE-conjugated secondary antibody (P2771MP, Thermo Fisher Scientific), and the dyes PKH-26 (Sigma-Aldrich) and Prolong Gold antifade reagent with DAPI (Invitrogen) were used for immunofluorescence microscopy. Apoptosis was induced with anti-Fas activating antibody (CH11, EMD Biosciences).

qPCR. qPCR analysis of transcript expression was performed by extracting total cellular RNA using an RNeasy kit (Qiagen). cDNA was prepared using the High Capacity cDNA Reverse Transcription Kit (Applied Biosystems), amplified with Fast SYBR Green Master Mix, and analyzed on a StepOne real time PCR system (Applied Biosystems). Fold changes were normalized to the expression levels of the house-keeping gene GAPDH. Primer pair sequences used for qPCR are listed in Supplemental Table 6.

Western blot. For Western blot analysis, cells were lysed in RIPA buffer supplemented with protease inhibitors (Roche Diagnostics) and a phosphatase inhibitor cocktail (EMD Biosciences). Proteins were separated by SDS-PAGE and transferred to a nitrocellulose membrane. Membranes were subsequently blocked with 5% nonfat dry milk or 5% BSA and probed with a mouse antibody specific to αSMA at 1:2000 (ab7817, Abcam) or the rabbit antibodies targeting caspase-3 (CASP3, 9662S), PARP (catalog 9532S), and GAPDH HRP conjugate (catalog 8884S) at 1:1000 (Cell Signaling Technologies). All experiments were performed in triplicate, and the results are presented as mean ± SEM.

Immunofluorescence microscopy. CCL210 fibroblasts were seeded and cultured in single-chamber slides (Nunc) followed by overnight serum starvation. Myofibroblasts were generated by incubation with TGF- β for 48 hours and were then treated with PGE₂ and/or FGF2 for an additional 5 days. Chamber slides were then washed twice with chilled PBS, fixed with freshly prepared 4% formaldehyde for 20 minutes, washed with PBS, and quenched with 100 mM glycine for 15 minutes. Blocking and permeabilization were achieved by incubating the slides for 1 hour in PBS containing 10% FBS and 0.1% Triton X-100 (Sigma-Aldrich). Cells were then incubated with either anti- α SMA-FITC (1:500) overnight at 4°C, anti-annexin V (1 μ g/mL) at 37°C for 1 hour followed by anti-rabbit PE-conjugated secondary antibody overnight at 4°C, or the membrane dye PKH26 (2 μ M) at room temperature for 3 minutes. Mounting medium containing DAPI was then used to stain the nuclei. Slides were examined using a Leica DC 500-fluorescence microscope equipped with a digital camera.

Proliferation and apoptosis assays. Lung myofibroblast proliferation studies were performed using the CyQUANT NF Cell Proliferation Assay Kit (Thermo Fisher Scientific). At the specified harvesting time, cells were detached with 0.25% trypsin and resuspended in HBSS containing CyQUANT NF dye reagent. Cell lysates were then transferred to a 96-well plate and incubated at 37°C for 45 minutes. Cell proliferation was measured by determining fluorescence in a microplate reader with excitation of 485 nm and emission of 530 nm. Lung myofibroblast apoptosis was evaluated following treatment with anti-Fas antibody at 100 ng/mL. Total and cleaved (active) forms of CASP3 and PARP were analyzed by Western blot. All experiments were performed in triplicate, and the results are presented as mean \pm SEM.

RNA-seq. For RNA-seq performed on in vitro specimens, CCL210 human adult lung fibroblasts were treated with PGE₂ or FGF2, or they were left untreated. Cells were harvested with Trizol followed by RNA extraction using the miRNeasy Mini kit (Qiagen), according to the manufacturer's protocol, and submitted for library prep and sequencing. For in vivo RNA-seq studies, fibroblasts were isolated from female FVB Col1 α 1-GFP transgenic mice — obtained from Derek Radisky (Mayo Clinic) — 30 days following bleomycin-challenge. Both young (2 months) and aged (18 months) mice were used in the study (80). Mouse lungs were digested and Col1 α 1-GFP⁺ fibroblasts were isolated by FACS. Total RNA was extracted using the RNeasy Micro Kit (Qiagen) according to manufacturer's protocol and submitted for library prep and sequencing. A detailed description of RNA library preparation, sequencing protocols, and analysis of RNA isolated from CCL210 and mouse fibroblasts is available in the supplement. Our RNA-Seq data were deposited in the NCBI GEO database (accession no. GSE163832).

Statistics. Statistical analysis was performed using GraphPad Prism software version 8.1.1. Experimental data are presented as means and were analyzed for statistical significance by 1-way ANOVA with the Tukey's multiple comparisons test, 2-way ANOVA (Figure 6B), or paired 2-tailed *t* test, as appropriate. *P* < 0.05 was considered significant. Data are presented as \pm SEM. For RNA-seq data, DESeq2 was used with default parameters to identify differentially expressed transcripts with cutoffs of Benjamini-Hochberg FDR-adjusted *P* < 0.05 and fold-change values (excluding small RNAs) of less than -1.5 or greater than 1.5 (81). We elected to omit fold-change cutoffs when analyzing small RNAs to capture all statistically significant changes that may have biologic relevance. Functional analysis of all RNAs (except small RNAs), including candidate pathways activated or inhibited in comparisons and GO-term enrichments (<http://www.geneontology.org/>), was performed using iPathway Guide (<http://www.advaitabio.com>) (82). See supplemental methods for detailed quality control and sequence alignment methodology.

Study approval. All animal experiments were carried out in accordance with the Mayo Clinic IACUC and conforming to the Animal Research: Reporting of In Vivo Experiments (ARRIVE) guidelines.

Author contributions

SMF, LRP, and MPG designed the in vitro experiments. TXP and GL designed the in vivo experiments. Experiments were performed by SMF, LRP, and TXP. Data were analyzed by SMF and DK. The manuscript was written by SMF and MPG.

Acknowledgments

We thank members of the Peters-Golden and Steven Huang labs for their valuable input into this work. We acknowledge support from the Bioinformatics Core of the University of Michigan Medical School's Biomedical Research Core Facilities and specifically thank Becky Tagett for her work on the small RNA-seq and analysis. This work was funded by the NIH grants RO1 HL094311 (to MPG), R35 HL144979 (to MPG), HL142596 (to GL), and 5T32HL007749-28 (to SMF).

Address correspondence to: Marc Peters-Golden, 6301 MSRB III, 1150 W. Medical Center Drive, Ann Arbor, Michigan 48109, USA. Phone: 734.936.5047; Email: petersm@umich.edu.

1. Wynn TA. Fibrotic disease and the T(H)1/T(H)2 paradigm. *Nat Rev Immunol*. 2004;4(8):583–594.
2. Wynn TA. Cellular and molecular mechanisms of fibrosis. *J Pathol*. 2008;214(2):199–210.
3. Fell CD, et al. Clinical predictors of a diagnosis of idiopathic pulmonary fibrosis. *Am J Respir Crit Care Med*. 2010;181(8):832–837.
4. Vaughan MB, et al. Transforming growth factor-beta1 promotes the morphological and functional differentiation of the myofibroblast. *Exp Cell Res*. 2000;257(1):180–189.
5. Penke LR, Peters-Golden M. Molecular determinants of mesenchymal cell activation in fibroproliferative diseases. *Cell Mol Life Sci*. 2019;76(21):4179–4201.
6. Thannickal VJ, Horowitz JC. Evolving concepts of apoptosis in idiopathic pulmonary fibrosis. *Proc Am Thorac Soc*. 2006;3(4):350–356.
7. Hinz B, Lagares D. Evasion of apoptosis by myofibroblasts: a hallmark of fibrotic diseases. *Nat Rev Rheumatol*. 2020;16(1):11–31.
8. Horowitz JC, Thannickal VJ. Mechanisms for the resolution of organ fibrosis. *Physiology (Bethesda)*. 2019;34(1):43–55.
9. Kato K, et al. Impaired myofibroblast dedifferentiation contributes to non-resolving fibrosis in aging. *Am J Respir Cell Mol Biol*. 2020;62(5):633–644.
10. Garrison G, et al. Reversal of myofibroblast differentiation by prostaglandin E(2). *Am J Respir Cell Mol Biol*. 2013;48(5):550–558.
11. Huang S, et al. Prostaglandin E(2) inhibits collagen expression and proliferation in patient-derived normal lung fibroblasts via E prostanoicid 2 receptor and cAMP signaling. *Am J Physiol Lung Cell Mol Physiol*. 2007;292(2):L405–L413.
12. Wettlaufer SH, et al. Reversal of the transcriptome by prostaglandin E2 during myofibroblast dedifferentiation. *Am J Respir Cell Mol Biol*. 2016;54(1):114–127.
13. Maltseva O, et al. Fibroblast growth factor reversal of the corneal myofibroblast phenotype. *Invest Ophthalmol Vis Sci*. 2001;42(11):2490–2495.
14. Koo HY, et al. Fibroblast growth factor 2 decreases bleomycin-induced pulmonary fibrosis and inhibits fibroblast collagen production and myofibroblast differentiation. *J Pathol*. 2018;246(1):54–66.
15. Narumiya S, et al. Prostanoid receptors: structures, properties, and functions. *Physiol Rev*. 1999;79(4):1193–1226.
16. Ornitz DM, Itoh N. The fibroblast growth factor signaling pathway. *Wiley Interdiscip Rev Dev Biol*. 2015;4(3):215–266.
17. Penke LR, et al. Prostaglandin E2 inhibits α -smooth muscle actin transcription during myofibroblast differentiation via distinct mechanisms of modulation of serum response factor and myocardin-related transcription factor-A. *J Biol Chem*. 2014;289(24):17151–17162.
18. Wettlaufer SH, et al. Distinct PKA regulatory subunits mediate PGE₂ inhibition of TGF β -1-stimulated collagen I translation and myofibroblast differentiation. *Am J Physiol Lung Cell Mol Physiol*. 2017;313(4):L722–L731.
19. Kolodick JE, et al. Prostaglandin E2 inhibits fibroblast to myofibroblast transition via E. prostanoid receptor 2 signaling and cyclic adenosine monophosphate elevation. *Am J Respir Cell Mol Biol*. 2003;29(5):537–544.
20. Stepp MW, et al. The c10orf10 gene product is a new link between oxidative stress and autophagy. *Biochim Biophys Acta*. 2014;1843(6):1076–1088.
21. Yoshida K, et al. MAP kinase activation and apoptosis in lung tissues from patients with idiopathic pulmonary fibrosis. *J Pathol*. 2002;198(3):388–396.
22. Nho RS, Hergert P. IPF fibroblasts are desensitized to type I collagen matrix-induced cell death by suppressing low autophagy via aberrant Akt/mTOR kinases. *PLoS One*. 2014;9(4):94616.
23. Lawrence J, Nho R. The role of the mammalian target of rapamycin (mTOR) in pulmonary fibrosis. *Int J Mol Sci*. 2018;19(3):E778.
24. Khalil N, Greenberg AH. The role of TGF-beta in pulmonary fibrosis. *Ciba Found Symp*. 1991;157:194–207.
25. Yue X, et al. TGF- β : titan of lung fibrogenesis. *Curr Enzym Inhib*. 2010;6(2).
26. Fernandez IE, Eickelberg O. The impact of TGF- β on lung fibrosis: from targeting to biomarkers. *Proc Am Thorac Soc*. 2012;9(3):111–116.
27. Hecker L, et al. NADPH oxidase-4 mediates myofibroblast activation and fibrogenic responses to lung injury. *Nat Med*. 2009;15(9):1077–1081.
28. Wernig G, et al. Unifying mechanism for different fibrotic diseases. *Proc Natl Acad Sci U S A*. 2017;114(18):4757–4762.
29. Eferl R, et al. Development of pulmonary fibrosis through a pathway involving the transcription factor Fra-2/AP-1. *Proc Natl Acad Sci U S A*. 2008;105(30):10525–10530.
30. Crestani B, et al. Hepatocyte growth factor and lung fibrosis. *Proc Am Thorac Soc*. 2012;9(3):158–163.
31. Marchand-Adam S, et al. Defect of hepatocyte growth factor secretion by fibroblasts in idiopathic pulmonary fibrosis. *Am J Respir Crit Care Med*. 2003;168(10):1156–1161.
32. Schaller MD. Cellular functions of FAK kinases: insight into molecular mechanisms and novel functions. *J Cell Sci*. 2010;123(Pt 7):1007–1013.
33. Hecker L, et al. Reversible differentiation of myofibroblasts by MyoD. *Exp Cell Res*. 2011;317(13):1914–1921.
34. Penke LR, et al. FOXM1 is a critical driver of lung fibroblast activation and fibrogenesis. *J Clin Invest*. 2018;128(6):2389–2405.
35. Huang SK, et al. Prostaglandin E2 inhibits specific lung fibroblast functions via selective actions of PKA and Epac-1. *Am J Respir Cell Mol Biol*. 2008;39(4):482–489.
36. Lama V, et al. Prostaglandin E2 synthesis and suppression of fibroblast proliferation by alveolar epithelial cells is cyclooxygenase-2-dependent. *Am J Respir Cell Mol Biol*. 2002;27(6):752–758.
37. Huang WT, et al. Plasminogen activator inhibitor 1, fibroblast apoptosis resistance, and aging-related susceptibility to lung fibrosis. *Exp Gerontol*. 2015;61:62–75.
38. Esteller M. Non-coding RNAs in human disease. *Nat Rev Genet*. 2011;12(12):861–874.
39. O'Reilly S. MicroRNAs in fibrosis: opportunities and challenges. *Arthritis Res Ther*. 2016;18:11.
40. Pandit KV, Milosevic J. MicroRNA regulatory networks in idiopathic pulmonary fibrosis. *Biochem Cell Biol*. 2015;93(2):129–137.
41. Hadjicharalambous MR, Lindsay MA. Idiopathic pulmonary fibrosis: pathogenesis and the emerging role of long non-coding RNAs. *Int J Mol Sci*. 2020;21(2):524.

42. Yu F, et al. NEAT1 accelerates the progression of liver fibrosis via regulation of microRNA-122 and Kruppel-like factor 6. *J Mol Med (Berl)*. 2017;95(11):1191–1202.
43. Huang S, et al. Long noncoding RNA MALAT1 mediates cardiac fibrosis in experimental postinfarct myocardium mice model. *J Cell Physiol*. 2019;234(3):2997–3006.
44. Savary G, et al. The long noncoding RNA DNM3OS is a reservoir of FibromiRs with major functions in lung fibroblast response to TGF- β and pulmonary fibrosis. *Am J Respir Crit Care Med*. 2019;200(2):184–198.
45. Huang C, et al. Long noncoding RNA FENDRR exhibits antifibrotic activity in pulmonary fibrosis. *Am J Respir Cell Mol Biol*. 2020;62(4):440–453.
46. Ouyang F, et al. Long non-coding RNA RNF7 promotes the cardiac fibrosis in rat model via miR-543/THBS1 axis and TGF β 1 activation. *Aging (Albany NY)*. 2020;12(1):996–1010.
47. Othman N, Nagoor NH. The role of microRNAs in the regulation of apoptosis in lung cancer and its application in cancer treatment. *Biomed Res Int*. 2014;2014:318030.
48. Gao Q, et al. Antifibrotic potential of MiR-335-3p in hereditary gingival fibromatosis. *J Dent Res*. 2019;98(10):1140–1149.
49. Nakashima T, et al. Impaired IL-17 signaling pathway contributes to the increased collagen expression in scleroderma fibroblasts. *J Immunol*. 2012;188(8):3573–3583.
50. Pang Q, et al. MicroRNA-152-5p inhibits proliferation and migration and promotes apoptosis by regulating expression of Smad3 in human keloid fibroblasts. *BMB Rep*. 2019;52(3):202–207.
51. Zhang Y, et al. let-7a suppresses liver fibrosis via TGF β /SMAD signaling transduction pathway. *Exp Ther Med*. 2019;17(5):3935–3942.
52. Yang S, et al. miR-145 regulates myofibroblast differentiation and lung fibrosis. *FASEB J*. 2013;27(6):2382–2391.
53. Huang Y, et al. MicroRNA-21: a central regulator of fibrotic diseases via various targets. *Curr Pharm Des*. 2015;21(17):2236–2242.
54. Cui H, et al. MicroRNA-27a-3p is a negative regulator of lung fibrosis by targeting myofibroblast differentiation. *Am J Respir Cell Mol Biol*. 2016;54(6):843–852.
55. Salmena L, et al. A ceRNA hypothesis: the Rosetta Stone of a hidden RNA language? *Cell*. 2011;146(3):353–358.
56. Li P, et al. Cytochrome c and dATP-dependent formation of Apaf-1/caspase-9 complex initiates an apoptotic protease cascade. *Cell*. 1997;91(4):479–489.
57. Moore BB, et al. Animal models of fibrotic lung disease. *Am J Respir Cell Mol Biol*. 2013;49(2):167–179.
58. Cabrera S, et al. Delayed resolution of bleomycin-induced pulmonary fibrosis in absence of MMP13 (collagenase 3). *Am J Physiol Lung Cell Mol Physiol*. 2019;316(5):L961–L976.
59. Caporarello N, et al. Vascular dysfunction in aged mice contributes to persistent lung fibrosis. *Aging Cell*. 2020(8):e13196.
60. Grosse R, et al. A role for VASP in RhoA-Diaphanous signalling to actin dynamics and SRF activity. *EMBO J*. 2003;22(12):3050–3061.
61. Jin J, et al. Pirfenidone attenuates lung fibrotic fibroblast responses to transforming growth factor- β 1. *Respir Res*. 2019;20(1):119.
62. Wolters PJ, et al. Pathogenesis of idiopathic pulmonary fibrosis. *Annu Rev Pathol*. 2014;9:157–179.
63. Zmajkovicova K, et al. The antifibrotic activity of prostacyclin receptor agonism is mediated through inhibition of YAP/TAZ. *Am J Respir Cell Mol Biol*. 2019;60(5):578–591.
64. Emelyanova L, et al. Impact of statins on cellular respiration and de-differentiation of myofibroblasts in human failing hearts. *ESC Heart Fail*. 2019;6(5):1027–1040.
65. Suzuki K, et al. Transcriptomic changes involved in the dedifferentiation of myofibroblasts derived from the lung of a patient with idiopathic pulmonary fibrosis. *Mol Med Rep*. 2020;22(2):1518–1526.
66. Micallef L, et al. The myofibroblast, multiple origins for major roles in normal and pathological tissue repair. *Fibrogenesis Tissue Repair*. 2012;5(Suppl 1):S5.
67. Schafer MJ, et al. Cellular senescence mediates fibrotic pulmonary disease. *Nat Commun*. 2017;8:14532.
68. Thannickal VJ, et al. Myofibroblast differentiation by transforming growth factor-beta1 is dependent on cell adhesion and integrin signaling via focal adhesion kinase. *J Biol Chem*. 2003;278(14):12384–12389.
69. Thomas PE, et al. PGE(2) inhibition of TGF-beta1-induced myofibroblast differentiation is Smad-independent but involves cell shape and adhesion-dependent signaling. *Am J Physiol Lung Cell Mol Physiol*. 2007;293(2):L417–L428.
70. Kopp F, Mendell JT. Functional classification and experimental dissection of long noncoding RNAs. *Cell*. 2018;172(3):393–407.
71. Ebert MS, Sharp PA. Roles for microRNAs in conferring robustness to biological processes. *Cell*. 2012;149(3):515–524.
72. Bozyk PD, Moore BB. Prostaglandin E2 and the pathogenesis of pulmonary fibrosis. *Am J Respir Cell Mol Biol*. 2011;45(3):445–452.
73. Guzy RD, et al. Fibroblast growth factor 2 is required for epithelial recovery, but not for pulmonary fibrosis, in response to bleomycin. *Am J Respir Cell Mol Biol*. 2015;52(1):116–128.
74. Lee JH, et al. Anatomically and functionally distinct lung mesenchymal populations marked by Lgr5 and Lgr6. *Cell*. 2017;170(6):1149–1163.
75. Habieli DM, Hogaboam CM. Heterogeneity of fibroblasts and myofibroblasts in pulmonary fibrosis. *Curr Pathobiol Rep*. 2017;5(2):101–110.
76. Zepp JA, et al. Distinct mesenchymal lineages and niches promote epithelial self-renewal and myofibrogenesis in the lung. *Cell*. 2017;170(6):1134–1148.
77. Bärnthaler T, et al. Inhibiting eicosanoid degradation exerts antifibrotic effects in a pulmonary fibrosis mouse model and human tissue. *J Allergy Clin Immunol*. 2020;145(3):818–833.
78. Andersson CR, et al. Mebendazole is unique among tubulin-active drugs in activating the MEK-ERK pathway. *Sci Rep*. 2020;10(1):13124.
79. Guerini AE, et al. Mebendazole as a candidate for drug repurposing in oncology: an extensive review of current literature. *Cancers (Basel)*. 2019;11(9):1284.
80. Caporarello N, et al. PGC1 α repression in IPF fibroblasts drives a pathologic metabolic, secretory and fibrogenic state. *Thorax*. 2019;74(8):749–760.
81. Love MI, et al. Moderated estimation of fold change and dispersion for RNA-seq data with DESeq2. *Genome Biol*. 2014;15(12):550.
82. Draghici S, et al. A systems biology approach for pathway level analysis. *Genome Res*. 2007;17(10):1537–1545.
83. Chen Q, et al. Long non-coding RNA PCAT-1 promotes cardiac fibroblast proliferation via upregulating TGF-beta1. *Eur Rev Med Pharmacol Sci*. 2019;23(23):10517–10522.

84. Xu W, et al. Long non-coding RNA PCAT-1 contributes to tumorigenesis by regulating FSCN1 via miR-145-5p in prostate cancer. *Biomed Pharmacother.* 2017;95:1112–1118.
85. Shang AQ, et al. Knockdown of long noncoding RNA PVT1 suppresses cell proliferation and invasion of colorectal cancer via upregulation of microRNA-214-3p. *Am J Physiol Gastrointest Liver Physiol.* 2019;317(2):G222–G232.
86. Tang PM, et al. LncRNAs in TGF- β -driven tissue fibrosis. *Noncoding RNA.* 2018;4(4):E26.
87. Jiang X, et al. LncRNA NEAT1 promotes hypoxia-induced renal tubular epithelial apoptosis through downregulating miR-27a-3p. *J Cell Biochem.* 2019;120(9):16273–16282.
88. Liao K, et al. Blocking lncRNA MALAT1/miR-199a/ZHX1 axis inhibits glioblastoma proliferation and progression. *Mol Ther Nucleic Acids.* 2019;18:388–399.
89. Han Y, et al. Hsa-miR-125b suppresses bladder cancer development by down-regulating oncogene SIRT7 and oncogenic long noncoding RNA MALAT1 [published online October 25, 2013]. *FEBS Lett.* <https://doi.org/10.1016/j.febslet.2013.10.023>.
90. Wang P, et al. LncRNA MEG3 enhances cisplatin sensitivity in non-small cell lung cancer by regulating miR-21-5p/SOX7 axis. *Onco Targets Ther.* 2017;10:5137–5149.
91. Braconi C, et al. microRNA-29 can regulate expression of the long non-coding RNA gene MEG3 in hepatocellular cancer. *Oncogene.* 2011;30(47):4750–4756.
92. Tang R, et al. LncRNA GAS5 attenuates fibroblast activation through inhibiting Smad3 signaling. *Am J Physiol Cell Physiol.* 2020;319(1):C105–C115.